Chemie der Erde 77 (2017) 81–93

Contents lists available at ScienceDirect

Chemie der Erde

journal homepage: www.elsevier.de/chemer

Geochemistry of S, Cu, Ni, Cr and Au-PGE in the garnet amphibolites from the Akom II area in the Archaean Congo Craton, Southern Cameroon

Beyanu Anehumbu Aye, Elisé Sababa, Paul-Désiré Ndjigui*

Department of Earth Sciences, University of Yaoundé 1, P.O. Box: 812, Yaoundé, Cameroon

ARTICLE INFO

Article history:
Received 19 October 2016
Received in revised form 16 January 2017
Accepted 17 January 2017
Editorial handling - Astrid Holzheid

Keywords:
Congo craton
Garnet amphibolites
Hydrothermal alteration
Weathering
Geochemistry
Base metals

ABSTRACT

The fresh and weathered garnet amphibolites, from the Akom II area in the Archaean Congo Craton, were investigated to determine the S, Cu, Ni, Cr, and Au-PGE values. The garnet amphibolites are composed of amphibole, plagioclase, garnet, quartz, and accessory apatite, spinel, sericite, pyrite, chalcopyrite and non-identified opaque minerals. The presence of apatite, sericite, and two generations of opaque minerals suggests that they might be affected by hydrothermal alteration. They are characterized by moderate Al_2O_3, Fe_2O_3, CaO, V, Zn, and Co contents with negative Eu- and Ce-anomalies. The sulfur concentrations are variable (380–1710 ppm). According to the sulfur contents, amphibolites can be grouped into two: amphibolites with low contents, ranging between 380 and 520 ppm (av. = 457 ppm); and amphibolites with elevated contents, varying from 1140 to 1710 ppm (av. = 1370 ppm). Amphibolites contain contrast amounts of Cu (~1800 to 5350 ppm) while nickel contents attain 121 ppm. Chromium contents vary from 43 to 194 ppm. Sulfur correlates positively with Cu and Cr, but negatively with Ni and Ni/Cr ratio. The total Au-PGE contents attain 59 ppb.

The presence of amphibole and feldspars confirms the low degree of amphibolite weathering. The secondary minerals are constituted of kaolinite, gibbsite, goethite and hematite. Despite the accumulation of some elements, the major and trace element distribution is quite similar to that of fresh amphibolites. Nevertheless, the weathering processes lead to the depletion of several elements such as S (239–902 ppm), Cu (520–2082 ppm), and Ni (20–114 ppm). Chromium and Au-PGE show an opposite trend marked by a slight enrichment in the weathered amphibolites. Amidst the Au-PGE, Pd (60 ppb) and Pt (23 ppb) have elevated contents in the fresh rocks as well as in the weathered materials. The PPGE contents are much higher than IPGE contents in both types of materials. The Pd/Pt, Pd/Rh, Pd/Ru, Pd/Ir, Pd/Os, and Pd/Au values indicate that Pt, Rh, Ru, Ir, Os and Au are more mobile than Pd. Chondrite-normalized base metal patterns confirm the abundance of Pd and the slight enrichment of Au-PGE in weathered rocks. Palladium, Rh and Ir are positively correlated with S. Conversely Pt and Ru are negatively correlated with S and Au is not correlated with S. Despite the high and variable S and Cu contents, the garnet amphibolites possess low Au-PGE and other base metals contents.

1. Introduction

Ultramafic rocks are the repository for platinum-group elements (PGE) (Satyanarayanan et al., 2011), as such, they contain the five largest PGE deposits worldwide viz.: (i) Merensky reef and (ii) UG2 chromitite reefs of Bushveld complex, South Africa; (iii) Main Sulfide zone of the Great Dyke, Zimbabwe; (iv) Johns-Manville (JM) reef of the Stillwater complex, USA; and (v) Noril'sk-Talnakh deposits, Russia (Cawthorn, 2005). The origin of PGE-mineralization in these large ultramafic intrusions is usually thought to be magmatic (Campbell et al., 1983). Mineralization within such intrusions emanates from elemental fractionation processes. This involves the preferential partitioning of the compatible platinum-group elements which have affinity for iridium (IPGE) from the incompatible platinum-group elements with high affinity for palladium (PPGE) within immiscible sulfide liquids. As a result, understandings of the origin of magmatic ore deposits are based on these fractionation processes (Lesher and Stone, 1996). Some mechanisms such as hydrothermal activities, metamorphism or weathering processes can modify the concentrations of several ele-

* Corresponding author.
E-mail address: lndjigui@yahoo.fr (P.-D. Ndjigui).

http://dx.doi.org/10.1016/j.chemer.2017.01.009
0009-2819/

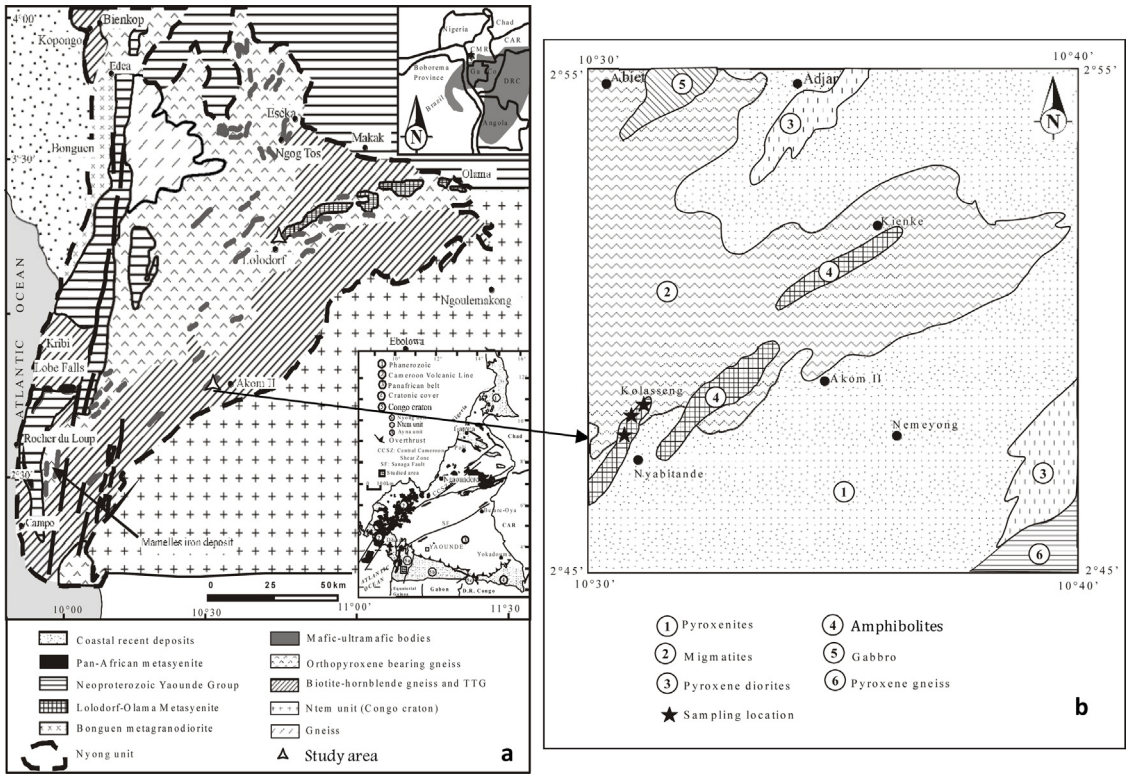

Fig. 1. a. Geological map of the Nyong unit (Lerouge et al., 2006). In the inset, the gray area represents the extent of the Congo and São Francisco cratons on Gondwana reconstruction; b. Geological map of the Akom II area (Champetier de Ribes and Aubague, 1956).

ments (e.g., S, Cu, Cr, Ni, and Au-PGE) from the initial magmatic rock (Prichard et al., 1986; Boudreau et al., 1986; Zaccarini et al., 2005; Wang et al., 2008; Ndjigui and Bilong, 2010). The weathered materials developed on ultramafic rocks have been proven to be characterized by comparatively higher contents that may go above 1000 ppm for Au-PGE (Traoré et al., 2008).

Several geochemical surveys for Ni, Cu, Au, and PGE have been carried out in Southern Cameroon on mafic-ultramafic rocks and their weathered products (e.g., Ndjigui et al., 2009; Ebah Abeng et al., 2012; Sababa et al., 2015). This shows high Ni contents in peridotites and moderate Pt and Pd contents in amphibolites. Palladium and Pt have the highest contents which attain 83 ppb and 26 ppb respectively. In the pyroxenites, Au-PGE contents are rather low (Ebah Abeng et al., 2012). Nevertheless, the sulfur contents have not been scrutinized in the mafic-ultramafic rocks. The sulfur saturation state in intrusive rocks is important for understanding distribution of chalcophile elements such as PGE because of the high sulphide liquid-silicate liquid partition coefficients for chalcophile elements such as PGE (Barnes and Maier, 1999; Shellnutt et al., 2015). This study is focused on geochemical investigation of S, Cu, Cr, Ni, and Au-PGE in the garnet amphibolites from the Akom II area within the greenstone belt in Southern Cameroon.

2. Regional geological setting

The Congo craton is a large sub-circular mass with a surface area of about 5711 000 km^2 (Shang et al., 2010). It is one of three large cratons which form the basement of the African continent. It outcrops in Central Africa and consists of several blocks of Archaean to mid Proterozoic age (Shang et al., 2007). The Congo craton is very well exposed in Southern Cameroon (Goodwin, 1991; Fig. 1a). It is represented by the Ntem group which forms the north western margin of the Archaean Congo craton. The Ntem complex comprises Mesoarchaean greenstone formations and dolerite dykes (Shang et al., 2010). This complex comprises from East to West three tectonic units based on their ages and lithology (Maurizot et al., 1986; Tchameni et al., 2004): Ntem, Nyong, and Ayina units (Fig. 1a).

The Ntem unit is Archaean in age and is subdivided: (i) Iron formations associated to amphibolites (Teutsong et al., 2017); (ii) The greenstone complexes (Maurizot et al., 1986; Ganno et al., 2015) (Fig. 1a and b). The garnet amphibolites of Akom II area belong to the Nyong unit. It corresponds to the northwestern remobilized and restructured border of Congo Craton (Maurizot et al., 1986; Penaye et al., 2004). The Nyong unit is made up of a foliated series and a greenstone belt (Ganno et al., 2017): (i) the foliated series include pyroxenites, migmatites, amphibolites and gneisses which outcrop enormously in the studied area (Fig. 1b). This series is intruded locally by mafic-ultramafic veins represented by gabbros, dolerites, and peridotites. The Nyong unit is cross-cut by the greenstone belt which is comprised of ferriferous quartzites, amphibolites, pyroxenites, leucocratic to mesocratic gneisses (Toteu et al., 1994; Fig. 1).

3. Sampling and analytical procedures

Nineteen samples were collected and crushed in the Department of Earth Sciences (University of Yaoundé 1, Cameroon). Thin sections were made in the University of Nancy (France) and in the Department of Applied Geosciences and Geophysics (University of Leoben, Austria). The observations under polarized light were done at the Department of Earth Sciences (University of Yaoundé 1) and under metallographic microscope at the Department of Applied Geosciences and Geophysics (University of Leoben).

The mineralogical and geochemical compositions were determined at the Geoscience Laboratories of the Ontario Geological Survey at Sudbury (Canada). The analytical procedures were previously described by several authors (e.g., Ebah Abeng et al., 2012; Sababa et al., 2015). The mineral assemblage for the weathered samples was identified by X-Ray Diffraction (XRD). X-Ray

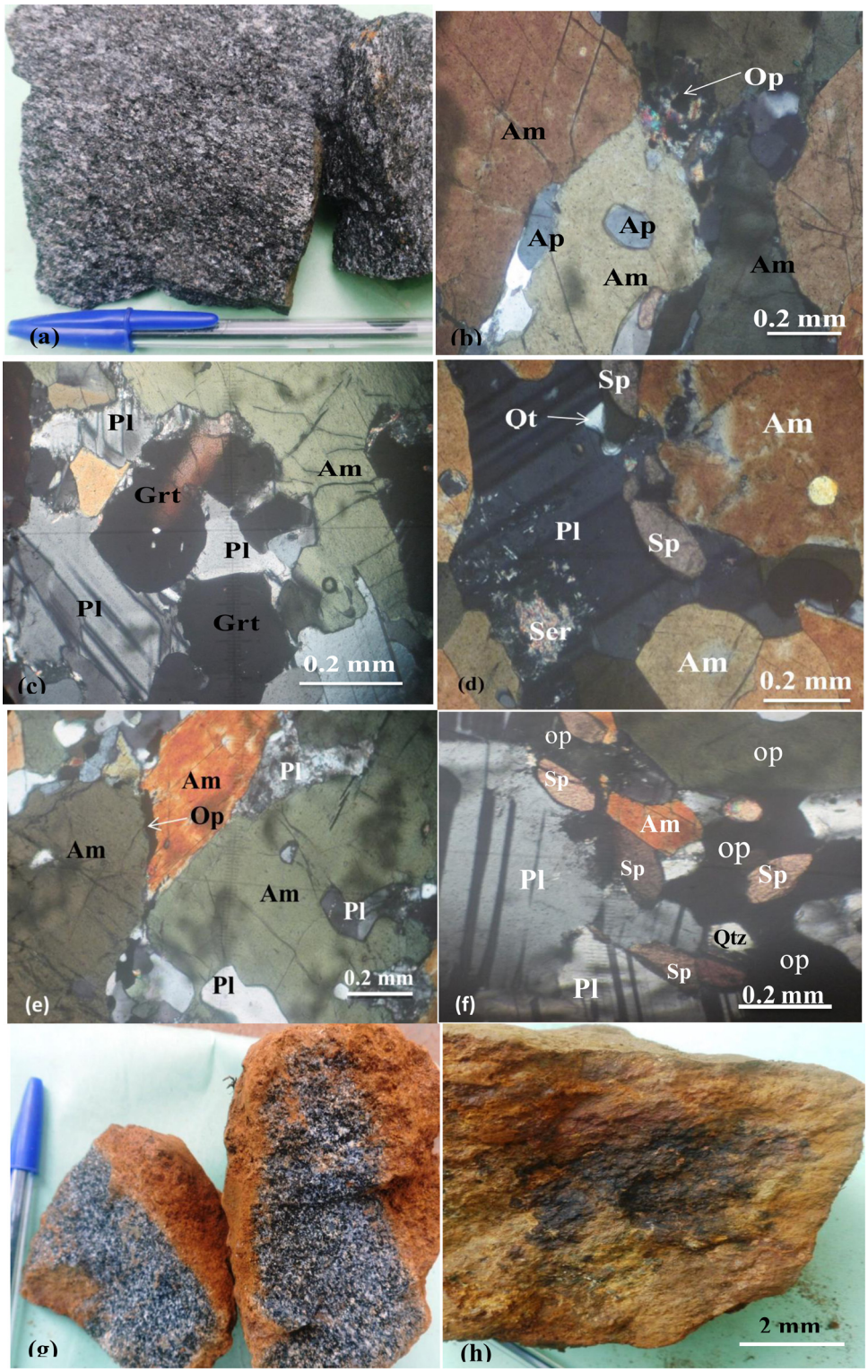

Fig. 2. Photographs and microphotographs of the selected samples: (a) photographs of the garnet amphibolite blocks; (b-f) photomicrographs of the garnet amphibolites (Am = amphibole; Ap = apatite; Op = opaque minerals; Pl = plagioclase; Grt = garnet; Ser: sericite; Sp: spinel); (g–h) photographs of the weathered amphibolites (g: large fresh core with red weathered rind; h: yellowish weathered block with black core). (For interpretation of the references to colour in this figure legend, the reader is referred to the web version of this article.)

Fluorescence (XRF) was used to determine the major element concentrations after sample ignition. Samples were prepared by acid dilution for the ICP-MS (Inductively Coupled Plasma-Mass Spectrometry) analyses for lithophile trace element concentrations by acid digestion in closed beakers.

Sulfur, Cu, and Au-PGE analyses were done in the Earth's Materials Laboratory at the University of Quebec at Chicoutimi (UQAC). Whole-rock sulfur was determined using an infrared HORIBA EMIA 220 V sulfur analyzer, using the method described by Bédard et al. (2008). The relative standard deviation is less than 5% for samples

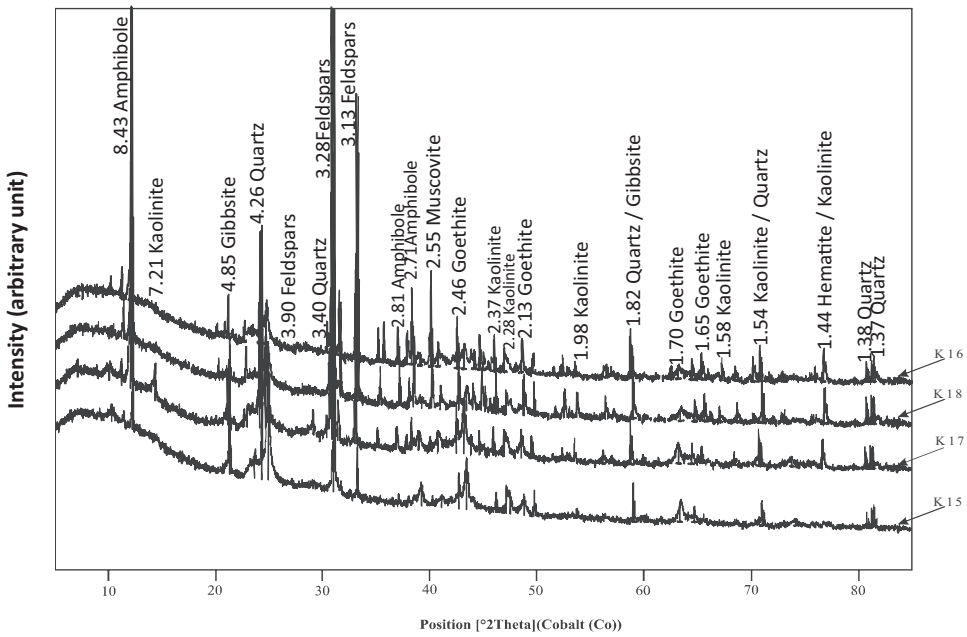

Fig. 3. X-ray patterns of four weathered materials (K15, K16, K17, and K18 samples).

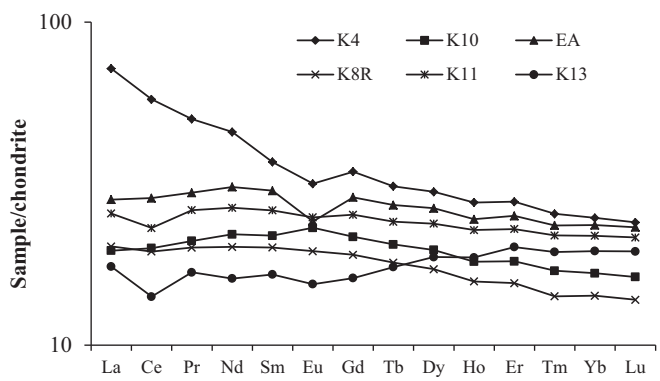

Fig. 4. Chondrite-normalized (McDonough and Sun, 1995) REE patterns for garnet amphibolites.

with S content more than 500 ppm. Copper was determined by atomic absorption spectrophotometry after aqua regia digestion. Au-PGE contents in the whole rock were determined by Ni-sulfide fire assay and Te co-precipitation followed by ICP-MS solution analysis using the technique described in Savard et al. (2010).

4. Results

4.1. Petrography

4.1.1. Petrography of fresh rocks

The garnet amphibolites are melanocratic and medium to coarse grained (Fig. 2a). The main minerals are amphibole (green hornblende ~55%), plagioclase (~18%), garnet (~15%), quartz (~5%), and accessory apatite, spinel, sericite, and opaque minerals. The crystal size of amphibole is microblast and phenoblast which can attain 2 mm in length. Some amphibolite crystals show micro-fractures which are progressively filled by opaque minerals (Fig. 2b). Plagioclase crystals present xenoblastic form of varied size (0.04–1 mm) (Fig. 2c). Plagioclase is often intermixed with quartz and spinel; it is partially replaced by sericite (Fig. 2d). Sericite forms from the alteration of plagioclase and appears as small scales or flakes (Fig. 2d). Garnet grains are porphyroblastic, globular with skeletal to sub rounded crystals and occur as inclusions in amphibole (Figs. 2c and d). Quartz occurs as microblast ranging from 0.06 to 0.3 mm in size and is usually xenoblastic and stretched. Apatite crystals occur as inclusion or in the interstices of amphibolites which recall a high-temperature hydrothermal process (Fig. 2b). Two generations of opaque minerals occur: the first occupies the interstices between mineral grains (Figs. 2d and e); and the second as xenoblast form of variable sizes with inclusions of spinel (Fig. 2f). The deformational features are suggestive of dynamic recrystallization due to hydrothermal alteration. The detailed observations under metallographic microscope show the presence of chalcopyrite and pyrite as opaque minerals.

4.1.2. Morphological and mineralogical features of weathered amphibolites

The weathered amphibolites outcrop as blocks with irregular forms under variable degree of weathering. They occur as isolated blocks in the weathered mantle of the surrounding formations and are zoned with a brownish weathered rim and dense massive fresh core (Fig. 2g) or are weathered with black core (Fig. 2h). The mineral assemblage is made up by amphibole, feldspars, quartz, kaolinite, and accessory gibbsite, goethite and hematite (Fig. 3). The processes of weathering involved here are hydrolysis and oxidation. The main hydrolysis processes of feldspars are monosiallitization and to a lesser extend allitization. Goethite and hematite result from the oxidation of the ferromagnesian silicate minerals such as amphibole. The presence of amphibole and feldspars is linked to the low degree of the weathering processes.

4.2. Geochemistry

4.2.1. Garnet amphibolites

The SiO_2 content of garnet amphibolites is in a range of a normal mafic rock (44–49 wt.%). Garnet amphibolites are characterized by moderate contents in Al_2O_3 (13–17 wt.%), Fe_2O_3 (14–20 wt.%), and CaO (8–10 wt.%). Apart from the above mentioned elements, other major elements have low contents (Table 1). Among the trace element suites, transition metals such as V, Zn, and Co have significant concentrations (Table 1). REE content varies between 41 and 112 ppm. The LREE/HREE ratio values that range from 1.49 to 3.21

Table 1
Distribution of major, trace and rare-earth elements in amphibolites.

	dl	K4	K10	EA	K8R	K11	K13
SiO_2 (wt.%)	0.04	48.38	49.49	49.12	48.14	44.68	49.17
Al_2O_3	0.02	14.43	17.21	14.16	14.32	14.63	13.25
Fe_2O_3	0.01	16.45	15.45	14.99	14.26	20.03	19.80
CaO	0.01	9.58	10.45	10.22	10.69	11.22	8.73
MgO	0.01	5.87	3.81	6.44	6.97	5.78	4.70
Na_2O	0.02	1.99	1.75	2.69	1.89	1.10	0.70
K_2O	0.01	0.71	0.11	0.35	0.26	0.12	0.11
MnO	0.01	1.74	1.31	1.65	1.01	1.75	1.85
P_2O_5	0.01	0.31	0.22	0.21	0.22	0.29	0.29
TiO_2	0.012	0.18	0.10	0.19	0.07	0.12	0.11
LOI	0.05	0.60	0.64	0.22	0.88	0.59	1.65
Total	–	100.26	100.53	100.27	98.73	100.32	100.27
Trace (ppm)	–						
V	0.8	335.5	314.7	248.4	327.4	>370	>370
Zn	1.8	130	84	111	103	130	100
Co	0.13	60.72	46.4	543.7	57.2	66.7	49.2
Sc	1.1	37.2	36.3	38.2	46.0	50.8	47.3
Ba	0.8	135.3	18.5	79.2	41.2	35.2	36.3
Zr	6	153	52	92	41	52	67
Sr	0.6	135.8	145.1	120.3	80.1	53.3	27
Y	0.05	43.3	26.9	37.5	23.2	33.4	26.8
Li	0.4	10.5	3.7	6.4	2.5	2.2	2
Ga	0.04	19	21.51	18.98	16.67	20.31	18.18
Nb	0.03	7.09	4.07	5.57	2.87	5.07	5.56
Hf	0.14	3.37	1.64	2.45	1.25	1.68	2.06
Mo	0.08	0.76	0.34	0.4	0.37	0.39	0.47
Th	0.02	2.86	0.51	0.74	0.32	0.56	0.63
U	0.01	0.83	0.16	0.19	0.13	0.15	0.19
Pb	0.18	2.4	1.4	0.8	1.5	1.1	2.1
Rb	0.11	15.24	2.8	7.92	2.69	2.04	3.58
Ta	0.01	0.46	0.28	0.36	0.20	0.35	0.38
Be	0.04	0.6	0.38	0.72	0.4	0.38	0.38
REE (ppm)							
La	0.10	17.00	4.65	6.69	4.79	6.06	4.15
Ce	0.12	35.33	12.24	17.48	11.905	14.13	8.67
Pr	0.01	4.65	1.95	2.75	1.86	2.43	1.56
Nd	0.06	20.89	10.07	14.11	9.21	12.17	7.35
Sm	0.03	5.46	3.23	4.45	2.97	3.87	2.45
Eu	0.01	1.78	1.30	1.36	1.10	1.40	0.87
Gd	0.01	6.85	4.31	5.71	3.79	5.04	3.21
Tb	0.01	1.12	0.74	0.98	0.65	0.87	0.63
Dy	0.01	7.34	4.85	6.53	4.23	5.85	4.61
Ho	0.01	1.51	0.99	1.34	0.86	1.24	1.02
Er	0.01	4.45	2.91	4.02	2.49	3.66	3.22
Tm	0.01	0.63	0.42	0.58	0.35	0.54	0.48
Yb	0.01	3.99	2.69	3.79	2.29	3.51	3.15
Lu	0.01	0.59	0.40	0.57	0.34	0.53	0.48
REE	–	111.509	50.75	70.36	46.88	61.30	41.85
LREE	–	85.11	33.44	46.84	31.88	40.06	25.05
HREE	–	26.48	17.31	23.52	15.00	21.24	16.80
LREE/HREEE	–	3.21	1.93	1.99	2.13	1.89	1.49
$(La/Yb)_N$	–	2.89	1.17	1.20	1.42	1.71	0.89
Ce/Ce^*	–	0.96	0.98	1.00	0.97	0.89	0.82
Eu/Eu^*	–	0.89	1.06	0.82	1.00	0.97	0.95

dl: detection limits.
$Ce/Ce^* = (Ce_{sample}/Ce_{chondrite})/(La_{sample}/La_{chondrite})^{1/2}(Pr_{sample}/Pr_{chondrite})^{1/2}$.
$Eu/Eu^* = (Eu_{sample}/Eu_{chondrite})/(Sm_{sample}/Sm_{chondrite})1/2(Gd_{sample}/Gd_{chondrite})^{1/2}$.
$(La/Yb)_N = (La_{sample}/La_{chondrite})/(Yb_{sample}/Yb_{chondrite})$.

exhibit the LREE-abundance relative to the HREE. The amphibolites from Akom II area are also characterized by low fractionation degree of REE revealed by the low $(La/Yb)_N$ ratio values (0.89-2.89) (Table 1). The chondrite-normalized (McDonough and Sun, 1995) REE patterns show (Fig. 4): (i) REE-enrichment compared to the chondrite values; (ii) flat REE patterns apart from sample K4 which confirms the LREE-enrichment; and (iii) slight negative Ce- and Eu-anomalies ($Ce/Ce^* = 0.82$; $Eu/Eu^* = 0.82$).

The concentrations of S, Cu, Ni, and Cr are listed in Table 2. According to the sulfur contents, garnet amphibolites have been subdivided into two groups: amphibolites with high S contents and amphibolites with moderate S contents. The high S contents range between 1140 and 1710 ppm (average = 1370 ppm) whereas the low ones are between 380 and 510 ppm with an average of 457 ppm. Average contents of Cu, Ni, and Cr are 3310, 89, and 109 ppm, respectively (Table 2). Ni/Cr ratios are variable with the average less than 1. Conversely, the Cu/(Cu + Ni) ratios are very close to 1 (Cu/(Cu + Ni) ~0.97) (Table 2). Sulfur correlates positively with Cu, Ni, and Cr (Fig. 5a–c) and negatively with Ni/Cr ratio (Fig. 5d).

The total PGE contents vary between 7 and 44 ppb. Palladium and Pt are the most abundant PGE (32.96 ppb for Pd and 13.18 ppb for Pt) (Table 2). The gold contents are up to 7.97 ppb. The total Au-PGE contents come up to 52 ppb. The garnet amphibolites are highly enriched in PPGE than IPGE (PPGE/IPGE = 11 ~ 84). They have higher

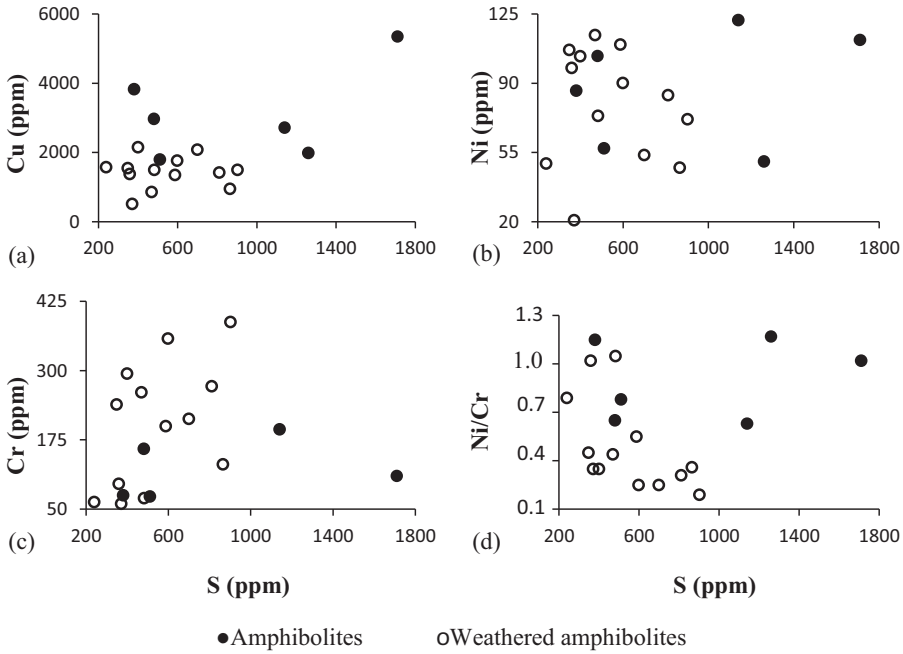

Fig. 5. Binary diagrams of sulfur vs. selected base metals: (a) S vs. Cu; (b) S vs. Ni; (c) S vs. Cr, (d) S vs. Ni/Cr.

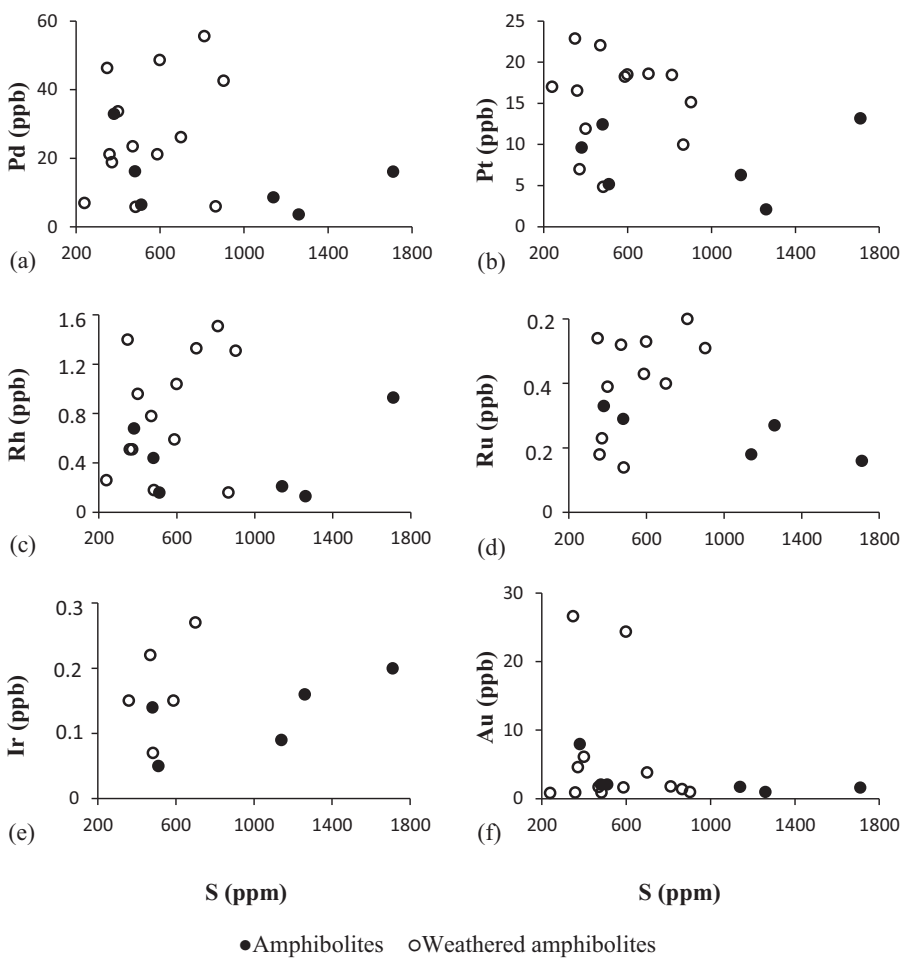

Fig. 6. Binary diagrams of sulfur vs. precious metals: (a) S vs. Pd; (b) S vs. Pt; (c) S vs. Rh, (d) S vs. Ru; (e) S vs. Ir; (f) S vs. Au.

Table 2
S. Cu, Ni, Cr, and Au-PGE concentrations and elemental ratios in garnet amphibolites.

	dl	with high S contents				with low S contents			
		K4	K10	EA	Av1	K8R	K11	K13	Av2
S (ppm)	–	1710	1260	1140	1370	480	380	510	457
Cu	–	5350	1990	2720	3353	2970	3830	1800	2867
Ni	1.6	111.9	50.5	121.9	94.77	103.8	86.3	57.1	82.4
Cr	3	110	43	194	116	159	75	73	102
Ni/Cr	–	1.02	1.17	0.63	0.94	0.65	1.15	0.78	0.86
Cu/(Cu + Ni)	–	0.98	0.98	0.96	0.97	0.97	0.98	0.97	0.97
Os (ppb)	0.07	<dl	0.10	0.11	0.11	0.19	<dl	<dl	0.19
Ir	0.03	0.20	0.16	0.09	0.15	0.14	<dl	0.05	0.10
Ru	0.12	0.16	0.27	0.18	0.20	0.29	0.33	<dl	0.31
Rh	0.08	0.93	0.13	0.21	0.42	0.44	0.68	0.16	0.43
Pt	0.08	13.18	2.11	6.28	7.19	12.45	9.63	5.18	9.09
Pd	0.47	16.11	3.64	8.63	9.46	16.21	32.96	6.50	18.56
Au	0.48	1.62	0.99	1.72	1.44	2.08	7.97	2.08	4.04
PGE	–	30.58	6.41	15.50	17.50	29.72	44.28	12.05	28.68
Au-PGE	–	33.82	8.39	18.94	20.38	31.80	51.57	13.97	32.45
Pd + Pt	–	29.29	5.75	14.91	16.65	28.66	42.59	11.68	27.64
Pd + Pt + Au	–	30.91	6.74	16.63	18.09	30.74	50.56	13.76	31.69
Pd/Pd + Pt	–	0.55	0.63	0.58	0.59	0.57	0.77	0.56	0.63
Au/Pd + Pt	–	0.06	0.17	0.12	0.12	0.07	0.19	0.18	0.15
IPGE	–	0.36	0.53	0.38	0.42	0.62	1.01	0.21	0.61
PPGE	–	30.22	5.88	15.12	17.07	29.10	43.27	11.84	28.08
PPGE/IPGE	–	83.94	11.09	39.79	44.94	46.94	42.84	56.38	48.72
Pd/Os	–	–	36.40	78.45	57.43	85.32	–	–	85.32
Pd/Ir	–	80.55	22.75	95.89	66.40	115.79	–	130.00	122.90
Pd/Ru	–	100.69	13.48	47.94	56.60	55.90	99.88	–	77.89
Pd/Rh	–	17.32	28.00	41.10	28.81	36.84	48.47	40.63	41.98
Pd/Pt	–	1.22	1.73	1.37	1.44	1.30	3.42	1.25	1.99
Pd/Au	–	9.94	3.68	5.02	6.21	7.79	4.14	3.13	5.02
Pd/(Pd + Pt)		0.55	0.63	0.58	0.57	0.57	0.77	0.56	0.63

dl: detection limits.
Av.: Average contents (n = 3).

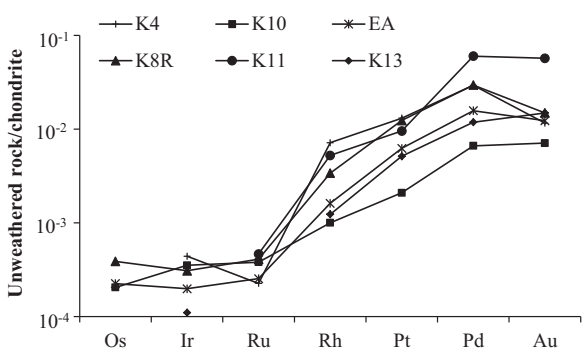

Fig. 7. Chondrite-normalized (McDonough and Sun, 1995) base metal (Au, PGE, Cr, Cu, and Ni) patterns for amphibolites.

Pd/Pt ratios (average Pd/Pt = 1.72) than the mantle (Pd/Pt = 0.53; Barnes et al., 1988). The Pd/Ir values are mostly higher (Pd/Ir = 1.74-130) than in the mantle (Pd/Ir = 1; Barnes et al., 1988). The Pd/Pt, Pd/Rh, Pd/Ru, Pd/Ir, Pd/Os, and Pd/Au values are higher than 1, indicating the high mobility of Ir, Ru, Rh, Os, Au and Pt relative to Pd (Table 2). The Pd/(Pd + Pt) values are low and constant (average Pd/(Pd + Pt) = 0.61) (Table 2). Sulfur has no correlation with Pd, Pt, and Rh (Figs. 6a–c), but is positively correlated with Ir (Fig. 6e) and negatively with Ru and Au (Fig. 6d and f).

The chondrite-normalized (McDonough and Sun, 1995) base metal patterns show a strong enrichment in Cu and Ni relative to Au-PGE; and an accumulation of Rh, Pt, Pd, and Au relative to Os, Ir, and Ru (Fig. 7).

4.2.2. *Weathered amphibolites*

SiO_2, Zn, REE contents of weathered amphibolites are lower than those of fresh samples. Conversely, Cr, V, Al_2O_3, Fe_2O_3 are accumulated in weathered amphibolites of Akom II area (Tables 3 and 4). The binary diagrams indicate negative correlations between SiO_2 and Al_2O_3, Fe_2O_3, MnO and Ti_2O (Fig. 8a–d), and positive correlations between SiO_2 and CaO, MgO, Na_2O and P_2O_5 (Fig. 8e-h). In addition, these diagrams reveal that Al, Fe, Mn and Ti are accumulated while Si, Ca, Mg, Na and P are leached during weathering processes. The lanthanide normalized spectra relative to chondrite (McDonough and Sun, 1995) reveal (Fig. 9; Table 3): (i) negative Eu-anomalies ($Eu/Eu^* \sim 0.75–0.86$); (ii) negative Ce-anomalies ($Ce/Ce^* \sim 0.58–0.83$); (iii) positive Ce-anomalies ($Ce/Ce^* \sim 1.22–4.08$); (iv) LREE-abundance relative to the HREE; (v) and low $(La/Yb)_N$ ratios that range between 0.95 and 6.80.

The weathered samples are also characterized by variable S and Cu contents. The S contents vary between 239 and 902 ppm (Table 4). Copper contents range from 520 to 2150 ppm. Nickel and Cr contents are low, ranging from 109-114 ppm for Ni, and 20–114 ppm for Cr. Average contents of S, Cu, Ni, and Cr in the weathered samples include 548, 1432, 79 and 204 ppm respectively (Table 4). Sulfur correlates positively with Cu (Fig. 5a); negatively with Ni (Fig. 5b); and positively with Cr (Fig. 5c). The negative correlation occurs also between sulfur and Ni/Cr ratio in the weathered amphibolites (Fig. 5d).

The Au-PGE contents are higher in weathered samples than in the fresh ones. The total PGE contents range between 11 and 93 ppb with Pt and Pd abundances (Table 4). The Au contents are very low and less than 1 ppb in three samples and up to 27 ppb in the others (Table 4). The total Au-PGE contents vary between 13 and 117 ppb. The weathered rocks are enriched in PPGE (16–77 ppb) than IPGE (0.26–2.11 ppb). The values of Pd/Pt, Pd/Ru, Pd/Ir, Pd/Rh and Pd/Au ratios can be used to disentangle the various mobilities of Au-PGE within weathered rocks (e.g., Bowles et al., 1994; Ndjigui and Bilong, 2010; Sababa et al., 2015). The Pd/Ru Pd/Ir, Pd/Rh, and Pd/Au ratios are greater than 1. This suggests that: (i) Ir, Ru, Rh and

Table 3
Distribution of major, trace and rare-earth elements in weathered amphibolites.

	dl	K1	K3	K6	K7	K17	K2	K9	K12	K14	K15	K16	K8W	K18
SiO_2 (wt.%)	0.04	26.71	37.08	49.11	34.26	38.29	38.14	48.55	47.49	25.3	28.74	45.22	37.15	42.25
Al_2O_3	0.02	24.17	16.53	13.15	15.35	18.48	16.73	15.93	14.50	21.49	19.95	14.34	16.69	15.65
Fe_2O_3	0.01	27.06	27.11	25.19	32.75	24.66	24.53	15.90	17.15	30.86	30.99	20.55	23.51	24.30
CaO	0.01	0.86	2.80	0.04	0.45	1.85	3.56	9.65	9.29	1.01	0.44	4.13	5.93	4.48
MgO	0.01	1.03	2.27	0.49	0.39	1.69	2.72	4.99	6.10	0.85	0.44	3.41	5.00	2.60
Na_2O	0.02	0.13	0.42	0.02	0.06	0.21	0.58	1.69	1.26	0.13	0.05	0.52	0.80	0.43
K_2O	0.01	0.69	0.24	0.81	0.41	0.21	0.19	0.17	0.17	0.15	0.30	0.32	0.24	0.41
MnO	0.01	2.79	2.02	1.96	2.93	1.88	2.52	1.34	1.28	3.25	2.98	1.76	1.59	2.68
P_2O_5	0.01	0.19	0.18	0.15	0.06	0.09	0.18	0.22	0.25	0.08	0.03	0.18	0.18	0.33
TiO_2	0.01	0.25	0.17	0.15	0.24	0.11	0.15	0.07	0.08	0.22	0.23	0.09	0.08	0.15
LOI	0.05	15.39	10.75	7.13	12.46	12.04	9.54	1.62	2.39	15.75	14.91	8.07	8.90	6.59
Total	–	99.31	99.63	99.24	99.38	99.56	98.89	100.11	99.96	99.14	99.10	98.63	100.11	99.87
Trace (ppm)	–													
V	0.8	>370	>370	103.6	>370	>370	>370	>370	355.6	>370	>370	353.0	>370	>370
Zn	1.8	54	71	51	38	71	98	100	105	45	35	68	91	155
Co	0.13	40.45	34.01	18.45	57.18	35.23	42.86	50.17	51.79	13.12	9.57	31.04	43.75	35.23
Sc	1.1	46.4	39.7	34.0	44.3	51.3	42.8	39.7	46.5	55.7	53.4	37.8	47.2	44.9
Ba	0.8	84.4	58.1	305.5	117.4	104.4	128.6	24.8	27.3	45.1	96.0	60.2	41.2	53
Zr	6	187	107	185	209	93	169	50	40	126	183	91	65	93
Sr	0.6	8.3	21	4.1	7.6	11.4	37.5	99	57.3	9.4	13.1	23.5	19	38.1
Y	0.05	4.87	13.42	1.7	3.53	6.23	16.54	20.17	20.69	5.12	7.57	14.84	10.26	18.11
Li	0.4	8.1	3.4	10.6	2.7	4.5	4.1	4.8	4.0	1.2	1.6	2.4	2.5	6.4
Ga	0.04	34.73	30.74	26.8	37.16	31.09	28.25	20.61	18.2	35.6	37.65	22.78	27.01	21.79
Pb	0.18	39.8	27.3	18	24.1	17.3	110.7	2.2	2.4	19.3	17.9	10.1	16.4	11.4
Rb	0.11	2.78	8.91	46.23	9.43	5.78	11.41	3.73	2.78	2.62	7.94	5.49	3.95	9.07
Nb	0.03	11.97	5.68	8.1	11.34	8.87	7.9	3.64	3.62	10.14	9.08	5.62	4.54	6.75
Hf	0.14	5.02	3.1	4.99	5.62	2.84	4.43	1.52	1.35	3.75	4.91	2.68	2.05	2.59
Mo	0.08	1.53	0.84	1.06	1.34	0.46	0.95	0.25	0.32	13.37	1.49	0.94	0.80	0.37
Th	0.02	3.68	1.44	1.7	6.71	1.82	1.83	0.57	0.45	1.67	1.58	2.35	1.40	2.82
U	0.01	1.24	0.67	1.01	1.59	0.9	0.78	0.16	0.14	0.73	0.86	0.71	0.52	0.86
Ta	0.01	0.77	0.39	0.42	0.8	0.69	0.51	0.24	0.25	0.63	0.56	0.39	0.31	0.45
REE (ppm)	–													
La	0.10	1.29	3.83	2.96	3.51	6.78	9.53	4.46	3.72	3.01	8.61	15.58	1.68	7.06
Ce	0.12	13.81	10.73	7.76	13.95	9.26	26.48	10.55	9.25	8.94	16.40	18.44	7.64	19.14
Pr	0.01	0.52	1.12	0.65	0.91	1.75	2.37	1.70	1.48	0.91	2.66	3.84	0.72	2.04
Nd	0.06	2.44	4.98	2.26	3.60	6.68	9.98	8.21	7.58	4.16	11.49	15.61	3.60	8.76
Sm	0.03	0.83	1.43	0.47	0.96	1.79	2.57	2.65	2.48	1.25	3.05	3.67	1.20	2.45
Eu	0.01	0.24	0.39	0.13	0.25	0.56	0.76	1.00	0.85	0.35	0.91	1.00	0.47	0.86
Gd	0.01	0.95	1.75	0.38	0.80	1.57	2.96	3.38	3.15	1.24	3.02	3.63	1.55	2.86
Tb	0.01	0.17	0.33	0.07	0.14	0.27	0.50	0.57	0.56	0.22	0.45	0.56	0.29	0.50
Dy	0.01	1.18	2.32	0.46	0.87	1.72	3.20	3.74	3.72	1.37	2.49	3.39	1.94	3.39
Ho	0.01	0.24	0.53	0.09	0.17	0.32	0.63	0.75	0.78	0.26	0.40	0.64	0.41	0.71
Er	0.01	0.80	1.70	0.30	0.50	0.96	1.83	2.24	2.34	0.75	1.00	1.81	1.26	2.12
Tm	0.01	0.13	0.26	0.06	0.08	0.15	0.26	0.31	0.34	0.11	0.14	0.27	0.18	0.31
Yb	0.01	0.92	1.82	0.44	0.58	1.05	1.67	2.06	2.32	0.78	0.86	1.77	1.19	2.03
Lu	0.01	0.15	0.27	0.07	0.09	0.15	0.25	0.31	0.34	0.11	0.12	0.25	0.18	0.29
REE	–	23.67	31.46	16.10	26.41	32.86	62.99	41.93	38.57	23.46	51.60	70.46	22.31	52.52
LREE	–	19.13	22.48	14.23	23.18	26.82	51.69	28.57	25.36	18.62	43.12	58.14	15.31	40.31
HREE	–	4.54	8.98	1.87	3.23	6.19	11.3	13.36	13.55	4.84	8.48	12.32	7.00	12.21
LREE/HREEE	–	4.21	2.50	7.61	7.18	4.33	4.57	2.14	1.87	3.85	5.08	4.72	2.19	3.30
Ce/Ce^*	–	4.08	1.25	1.35	1.89	0.65	1.35	0.93	0.95	1.31	0.83	0.58	1.68	1.22
Eu/Eu^*	–	0.82	0.75	0.94	0.87	1.02	0.84	1.02	0.93	0.86	0.91	0.84	1.05	0.99
$(La/Yb)_N$	–	0.95	1.43	4.57	4.11	4.39	3.88	1.47	1.09	2.62	6.80	5.98	0.96	2.36

dl: detection limits.
$Ce/Ce^* = (Ce_{sample}/Ce_{chondrite})/(La_{sample}/La_{chondrite})^{1/2}(Pr_{sample}/Pr_{chondrite})^{1/2}$.
$Eu/Eu^* = (Eu_{sample}/Eu_{chondrite})/(Sm_{sample}/Sm_{chondrite})^{1/2}(Gd_{sample}/Gd_{chondrite})^{1/2}$.
$(La/Yb)_N = (La_{sample}/La_{chondrite})/(Yb_{sample}/Yb_{chondrite})$.

Au are more mobile than Pd in the weathered amphibolites; (ii) Ir is highly mobile compared to other Au-PGE; (iii) Ru is more mobile than Rh which is in turn more mobile than Au; (iv) Pt is slightly more mobile than Pd, except for K7 and K18 samples (Table 4). However, the Pd/Pt values are higher than 1 in certain samples. This indicates the contrast Pt behavior during the weathering processes (Table 4). Palladium, Rh, Ru and Ir are positively correlated with S (Fig. 6a, c, d and e). Conversely, the correlation is negative between platinum and sulfur (Fig. 6b).

The chondrite-normalized (McDonough and Sun, 1995) base metal patterns reveal the abundance of Cu, Pd and Ni in the weathered amphibolites (Fig. 10a). The chondrite-normalized (McDonough and Sun, 1995) patterns for average contents of the weathered and fresh rocks follow the same trends and reveal the slight enrichment in PGE probably caused by low degree of amphibolite weathering (Fig. 10b). As for the fresh rocks, Os, Ir and Ru are depleted (Fig. 10a and b). In fact, PPGE are more mobile than IPGE during the early stage of weathering. This suggests that the processes that lead to PGE-, Ni- and Cu-abundance are quite different.

Gold, Ru, Rh, Pt, Pd, and Cr are positively correlated in the Grant's isocon diagram (Grant, 1986, 2005), which is used to graphically identify the most immobile elements (Fig. 11). The diagram con-

Table 4
S, Cu, Ni, Cr, and Au-PGE contents in the weathered amphibolites.

	dl	K1	K3	K6	K7	K17	K2	K9	K12	K14	K15	K16	K8W	K18	Av.
S (ppm)	–	699.45	598.04	370.72	865.06	586.91	399.55	482.61	358.52	902.18	810.58	348.03	469.13	239.15	548
Cu	–	2082	1770	520	950	1350	2150	1500	1380	1500	1420	1550	860	1580	1432
Ni	1.6	53.8	90.1	20.8	47.3	109.6	103.7	73.5	97.7	71.8	84	106.9	114.3	49.5	789
Cr	3	213	358	60	131	200	295	70	96	388	272	239	261	63	204
Ni/Cr	–	0.25	0.25	0.35	0.36	0.55	0.35	1.05	1.02	0.19	0.31	0.45	0.44	0.79	0.49
Cu/(Cu + Ni)	–	0.97	0.95	0.96	0.95	0.92	0.95	0.95	0.93	0.95	0.94	0.93	0.88	0.97	0.94
Os (ppb)	0.07	<dl	<dl	<dl	<dl	0.19	<dl	0.07	0.15	<dl	<dl	<dl	0.22	<dl	0.16
Ir	0.03	0.27	<dl	<dl	<dl	0.15	<dl	0.07	0.15	<dl	<dl	<dl	0.22	<dl	0.17
Ru	0.12	0.40	0.53	0.23	<dl	0.43	0.39	0.14	0.18	0.51	0.60	0.54	0.52	<dl	0.41
Rh	0.08	1.33	1.04	0.51	0.16	0.59	0.96	0.18	0.51	1.31	1.51	1.40	0.78	0.26	0.81
Pt	0.08	18.58	18.51	6.99	9.98	18.24	11.90	4.85	16.53	15.12	18.44	22.87	22.04	17.00	15.47
Pd	0.47	26.14	48.61	18.79	5.95	21.14	33.64	5.79	21.16	42.57	55.59	46.31	23.45	6.94	27.39
Au	0.48	3.80	24.34	4.58	1.38	1.62	6.07	0.89	0.88	0.95	1.75	26.59	1.68	0.80	5.79
PGE	–	46.72	68.69	26.52	16.09	40.74	46.89	11.10	38.68	59.51	76.14	71.12	47.23	24.20	44.13
Au-PGE	–	50.52	93.03	31.10	17.47	42.36	52.96	11.99	39.56	60.46	77.89	97.71	48.91	25.00	49.92
IPGE	–	0.67	0.53	0.23	–	0.77	0.39	0.28	0.48	0.51	0.60	0.54	0.96	–	0.54
PPGE	–	46.05	68.16	26.29	16.09	39.97	46.50	10.82	38.20	59.00	75.54	70.58	46.27	24.20	43.67
PPGE/IPGE	–	68.73	128.60	114.30	–	51.91	119.23	38.64	79.58	115.69	125.90	130.70	48.19	–	92.86
Pd/Pt	–	1.42	2.63	2.69	0.60	1.16	2.83	1.19	1.28	2.82	3.01	2.02	1.06	0.41	1.78
Pd/Ir	–	96.81	–	–	–	–	–	82.71	141.07	–	–	–	106.59	–	106.80
Pd/Os	–	–	–	–	–	111.26	–	82.71	141.07	–	–	–	106.59	–	110.41
Pd/Ru	–	65.35	91.72	81.70	–	49.16	86.26	41.36	117.56	83.47	92.65	85.76	45.10	–	76.37
Pd/Rh	–	19.65	46.74	36.84	37.19	35.83	35.04	32.17	41.49	32.50	36.81	33.08	30.06	26.69	34.16
Pd/Au	–	6.88	2.00	4.10	4.31	13.05	5.54	6.51	24.05	44.81	31.77	1.74	13.96	8.68	12.88

dl: detection limits.
Av. = Average contents (n = 13).

firms PGE-abundance in the weathered samples revealed by the chondrite-normalized base metal patterns (Fig. 10b). Osmium, Ir, Au, Ru Rh, Pt, Pd, and Cr show enrichment while Ni, Cu and S are slightly depleted (Fig. 11).

5. Discussion

5.1. Petrography and geochemistry of fresh rocks

The garnet amphibolites from Akom II area are derived from mafic igneous rocks and result from a prograde metamorphism (Ebah Abeng et al., 2012). The presence of sulfide minerals (chalcopyrite and pyrite), sericite and to a lesser extent apatite in garnet amphibolites suggest that they might be affected by hydrothermal events (Sharrad et al., 2014). Meanwhile, Si, Al, Fe, Ca, Cr, V, Zn, Ni, Cu, and Co have significant contents. The geochemical data confirm the mafic nature of rocks. The low LREE/HREE ratios could be related to the partial melting phenomena of source protoliths (Bilong et al., 2011) with garnet among the residual phases (Nzenti et al., 2006). The sample K4 with high LREE contents may not experience these phenomena. The negative Eu-anomalies could be linked to the plagioclase fractionation (Lee et al., 2009) while the negative Ce-anomalies might reflect removal of Ce during hydrothermal alteration.

The sulfur content of the investigated rocks could also be related to the S contents of the silicate magma (Wallace and Carmichael, 1992). Hydrothermal events affected the distribution of sulfur. Thus, the low sulfur contents may be due to a first episode of hydrothermal activities. However the relatively higher sulfur values (1705 ppm) suggest another episode of hydrothermal activities rich in S (Puchtel et al., 1995).

The samples that have undergone the maximum sulfur removal are not necessarily those that have the highest PGE and other base metal contents. These observations imply that the processes that triggered the S removal and the PGE and base metal enrichment or remobilization are probably distinct (Godel and Barnes, 2007; Godel et al., 2007). Otherwise, direct measurement of sulfur contents in samples has in many cases been considered unreliable because of the volatile and mobile nature of S which is lost during magma degassing or low temperature alteration (e.g., Bai et al., 2012; Naldrett et al., 2012). The high Cu contents are also associated to different episodes of the hydrothermal activities (Zhou et al., 2004) and might also result to the presence of chalcopyrite ($CuFeS_2$) (Godel et al., 2007). The low Ni contents and the Ni/Cr values may reflect the lack of Ni-bearing minerals like olivine in garnet amphibolites (Sababa et al., 2015). In addition, Ir, Pd and Cu are strongly partitioned into sulphide phases compared to Ni, Cu and Zr, respectively, under S-saturated conditions (Shellnutt et al., 2015). The mineralization episodes may be syn-metamorphic in origin or alternatively, they are part of a pre-metamorphic event and underwent recrystallization during metamorphism (Sharrad et al., 2014).

Garnet amphibolites are richer in Pd, Pt, and Au compared to other mafic-ultramafic rocks (Gueddari et al., 1994; Ebah Abeng et al., 2012; Sababa et al., 2015). Palladium, Pt, and Au might be concentrated in the amphibolites by ascending hydrothermal fluids (Naldrett et al., 2008). Alard et al. (2000) showed that during partial melting of the mantle, base metal sulfides (BMS) melt incongruently to produce Cu-Ni-rich sulfide melt that concentrates Pd and Pt. Godel and Barnes (2007) explained the high Pd and to a lesser extent Pt enriched samples (high Pd/Pt or Pd/Ir ratios, e.g., K13). According to Godel and Barnes (2007), during hydrothermal process, a new fluid percolated through the cumulate pile and removed Pd and Pt from the footwall. As the fluid migrated, it could have reacted with the sulfides and precipitated Pd and Pt in the microfractures. This similar signature suggests that the high Pd and Pt contents in garnet amphibolites could have been leached out from other sources. This may also suggest that Pd could be distributed in sulfide minerals (Pašava et al., 2010) or transported as bisulfide complexes in acidic-neutral solutions under reduced and moderate oxidation conditions at 300 °C (Barnes and Liu, 2012) and disseminated in the whole rocks. The garnet amphibolites present overall low Au-PGE contents which often attain only tens of ppb, particularly low Os, Ir, Ru, and Rh contents. These contents are similar to other findings on Au-PGE in Southern Cameroon (Ebah Abeng et al., 2012). The depletion of Au-PGE could result from the mobility of PGE during hydrothermal alteration (Ahmed et al., 2009). The PGE data confirms the heterogeneity of PGE distribution in the Earth's

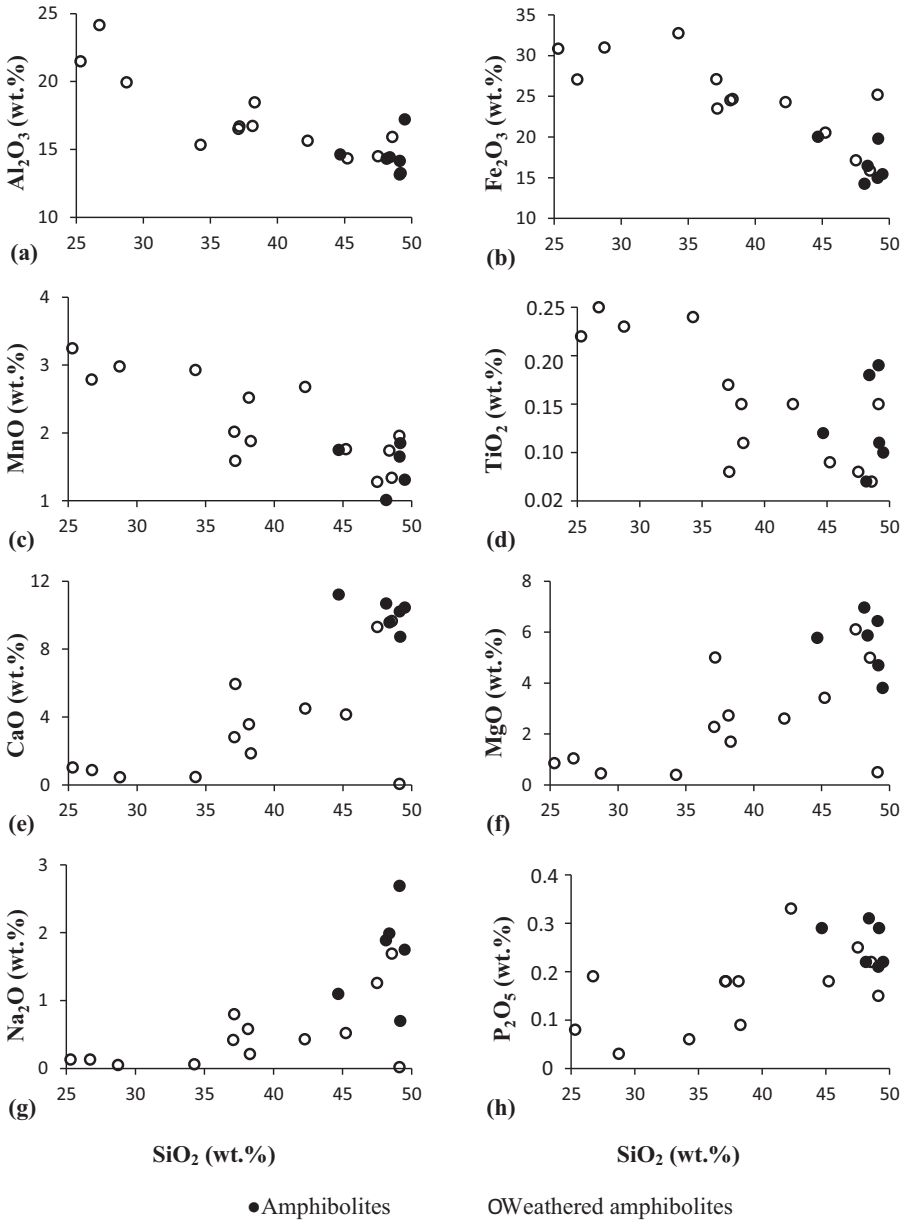

Fig. 8. Binary diagrams of major elements: (a) SiO_2 vs. Al_2O_3; (b) SiO_2 vs. Fe_2O_3; (c) SiO_2 vs MnO; (d) SiO_2 vs TiO_2; (e) SiO_2 vs. CaO; (f) SiO_2 vs. MgO; (g) SiO_2 vs. Na_2O; (h) SiO_2 vs. P_2O_2.

mantle (Xu et al., 1998). The low PGE contents suggest that the garnet amphibolites formed from the silicate magma that had already experienced prior-sulfide separation (Song et al., 2009), or the low proportion of PGE-carriers (Lorand and Alard, 2001) or to the depletion during hydrothermal events (Satyanarayanan et al., 2011; Hao et al., 2014).

Garnet amphibolites are enriched in PPGE over IPGE. According to Ahmed et al. (2009) and Ismail et al. (2010), the high difference in the contents of PPGE and IPGE may be due to PGE fractionation. The low Ir, Ru, and Rh contents could be due to their extremely limited hydrothermal mobility (Barnes and Liu, 2012). The high PPGE enrichment is possibly due to partial melting of the upper mantle under ultra-high temperature metasomatic conditions. The fact that the rocks are poor in IPGE compared to Pt and Pd show that Pt and Pd were enriched by hydrothermal fluids, since the IPGE are considered as relatively immobile in fluids compared to Pt and Pd (Mountain and Wood, 1988; Hsu et al., 1991; Fleet and Wu, 1993).

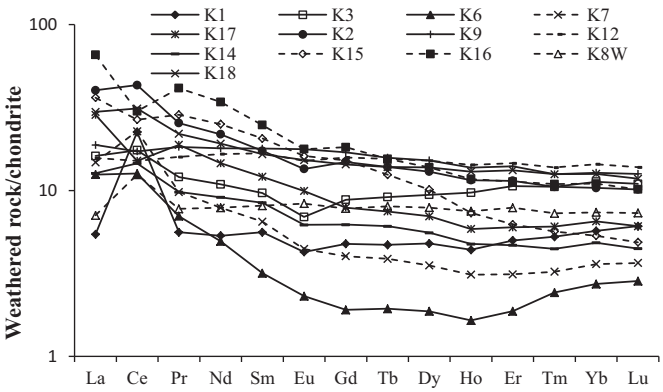

Fig. 9. Chondrite-normalized (McDonough and Sun, 1995) REE patterns for weathered amphibolites.

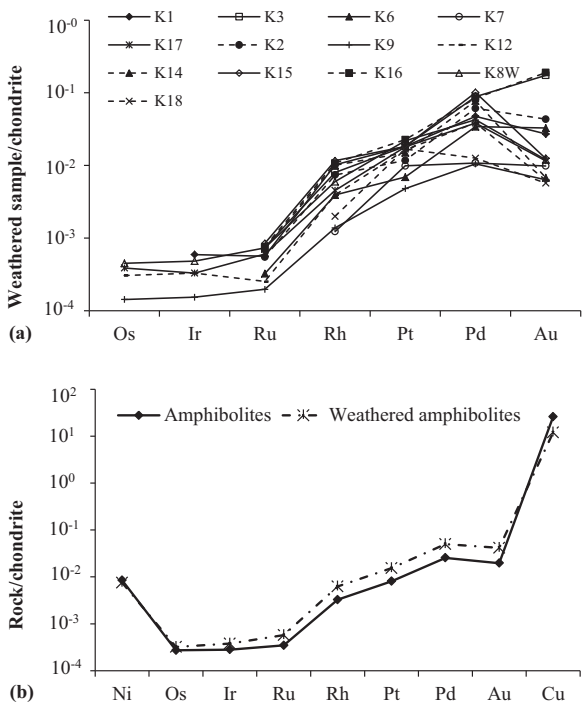

Fig. 10. Chondrite-normalized (McDonough and Sun, 1995) base metal patterns for: (a) weathered amphibolites; and (b) average contents for the fresh and weathered samples.

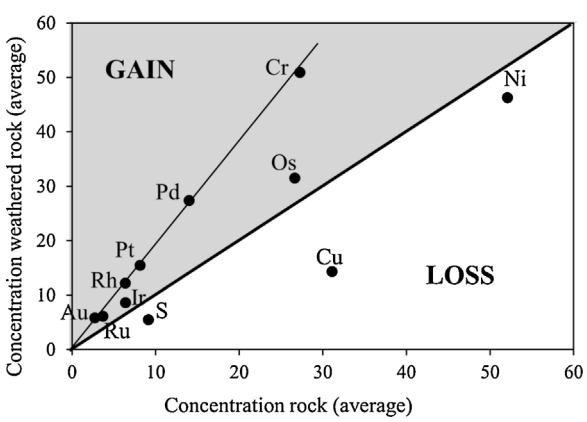

Fig. 11. Grant diagrams of weathered samples vs. amphibolites. The diagrams are constructed for S, Cu in ppm/100, Ni in ppm/1.7, Cr in ppm/4, Os in ppb*200, Ir in ppb/50, Ru, Rh in ppb*15, Pt, Pd and Au in ppb.

The high Pd/Ir ratios confirm a hydrothermal origin (Bleeker, 1990). The positive correlation between S and iridium (Fig. 3f) does not hold for any of the other PGE or Cu. This would seem to indicate that iridium is not fractionated from sulfur minerals under a wide range of conditions that lead to the mobilization sulfides in the rock (Good and Naldrett, 1993). The contrast behavior of Au-PGE and S seems to indicate that the garnet amphibolites were affected by another hydrothermal episode deposition containing PGE in the greenstone belt of Southern Cameroon. The garnet amphibolites from the greenstone belt are enriched in Pd and Cu, and depleted in Ni and Ir, similarly to that of the Proterozoic Donaldson West and Katiniq deposits of the Cape Smith belt (Good and Naldrett, 1993). The amphibolites of the Akom II area in the greenstone belt exhibit more fractionated Pd/(Pd + Pt) and Cu/(Cu + Ni) ratios than those of the Thompson belt (Good and Naldrett, 1993). However, both belts show similar less fractionated Pd/Ir ratios (Good and Naldrett, 1993).

5.2. Petrography and base metal geochemistry of weathered amphibolites

The macroscopic aspects of the weathered blocks and the presence of primary minerals such as amphibole and feldspars indicate that the garnet amphibolites of Akom II area are in the early stage of the weathering processes (Delvigne, 1998). This is confirmed by the fresh core of several weathered samples. The low contents in several major and trace elements such as Si, Ca, Mg, Na, P Zn, REE are characteristic of weathering processes (Beauvais, 2009). The accumulation of Al, Fe, Mn, Ti, Cr and V might be linked to the stability of newly crystalline secondary minerals like kaolinite, gibbsite, and goethite (Manceau et al., 2000; Singh et al., 2002). The positive and negative Ce-anomalies could result from the variability of oxidizing conditions (Neal and Taylor, 1989). The negative Eu-anomalies could be inherited from the fresh rocks or due to the weathering of plagioclase.

The higher PGE contents could be due to the presence of goethite in which PGE can be trapped (Wimpenny et al., 2007). The IPGE/PPGE values are also higher in weathered rocks than in the fresh ones. This is due to the high mobility of PPGE during weathering processes (Cabral et al., 2007). The relative high IPGE contents might be caused by the low degree of weathering (Auge and Legendre, 1994; Fonseca et al., 2009). The negative correlation between S and Ni, and S with Ni/Cr reveals the opposite behavior of both base metals during the weathering processes contrary to the correlation between S and Ir. Sulfur and iridium are highly leached in the supergene environment.

The positive correlation of Au, Ru, Rh, Pt, Pd, and Cr in the Grant's isocon diagram suggests that these base metals have similar behavior during the weathering processes. The depletion in Ni, Cu and S means that they are more soluble in their oxidized form. Conversely, Os, Ir, Au, Ru Rh, Pt, Pd, and Cr are less soluble in their oxidized form too (Berger et al., 2015). According to Fu et al. (2015), the accumulation of Au-PGE in weathered samples could be strongly linked to the presence of organic matter.

The fresh and weathered garnet amphibolites from the Akom II area have very similar geochemical features for base metals (S, Cu, Ni, and Au-PGE). These materials are at their early stage of weathering and are not too differentiated despite their variable S contents. According to several authors (e.g., Cabral et al., 2007; Suarez et al., 2010; Ndjigui and Bilong, 2010; Ebah Abeng et al., 2012; Sababa et al., 2015), platinum-group elements are also remobilized in geological materials in their early stage of weathering.

6. Conclusions

1. The garnet amphibolites are composed of amphibole, plagioclase, garnet, quartz, and accessory apatite, spinel, sericite, pyrite, chalcopyrite, and non-identified opaque minerals. Hydrothermal alteration leads to dynamic recrystallization.
2. The geochemical features which are depleted in many major and trace elements including REE are those of basic rocks. Garnet amphibolites are characterized by negative Eu- and Ce-anomalies.
3. The S contents are variable in the fresh rocks. The amphibolites have high Cu and low Au-PGE contents. The low Ni contents are linked to the absence of Ni-bearing minerals.
4. The weathered samples have low Si, Ca, Mg, Na, P, Zn, REE contents and high Al, Fe, Mn, Ti, Cr, and V contents compared to the fresh materials. The Grant's isocon diagram confirms the Au-PGE abundance and reveals that Au, PPGE, and Cr are the most immobile elements.

5. The hydrothermal alteration infers the leaching of several elements. Thus, sulfur, nickel and Au-PGE are not enriched enough to form workable deposits.

Acknowledgements

The authors are grateful to Professor Sarah-Jane Barnes for funding the sulfur and Au-PGE analysis at LabMaTer (UQAC). The whole rock analyses were partly financed by the GeoLabs (Sudbury, Canada), including sample preparation and laboratory analyses. We also appreciate the team of Earth's Materials Laboratory of University of Quebec at Chicoutimi (UCAC, Canada), for their advice. The authors are grateful to the members of the Department of Applied Geosciences of the University of Leoben (Austria) for thin section observations under metallographic microscope. The constructive comments by the associated editor (Prof. Astrid Holzheid) and two anonymous reviewers are highly appreciated.

References

Ahmed, H.A., Shoji, A., Yaser, M.A.-A., Moha, I., Abdellatif, R., 2009. Platinum-group elements distribution and spinel composition in podiform chromitites and associated rocks from the upper mantle section of the Neoproterozoic Bou Azzer ophiolite, Anti-Atlas Morocco. J. Afr. Earth Sci. 55, 92–104.

Alard, O., Griffin, W.L., Lorand, J.P., Jackson, S.E., O'Reilly, S.Y., 2000. Nonchondritic distribution of the highly siderophile elements in mantle sulphides. Nature 407, 891–894.

Auge, T., Legendre, O., 1994. Platinum-group element oxides from the Pirogues ophiolitic mineralization, New Caledonia: origin and significance. Econ. Geol. 89, 1454–1468.

Bédard, L.P., Savard, D.D., Barnes, S.-J., 2008. Total sulphur concentration in geological reference materials by elemental infrared analyzer. Geostand. Geoanal. Res. 32, 203–208.

Bai, Z.-J., Zhong, H., Li, C., Zhu, W.-G., Xu, G.-W., 2012. Platinum-group elements in the oxide layers of the Hongge mafic-ultramafic intrusion, Emeishan Large Igneous Province, SW China. Ore Geol. Rev. 46, 149–161.

Barnes, Stephan J., Liu, W., 2012. Pt and Pd mobility in hydrothermal fluids: evidence from komatiites and from thermodynamic modelling. Ore Geol. Rev. 44, 49–58.

Barnes, S.-J., Maier, W.D., 1999. The fractionation of Ni, Cu and the noble metals in silicate and sulphide liquids. In: Keays, R.R., Lesher, C.M., Lightfoot, P.C., Farrow, C.E.G. (Eds.), Dynamic Processes in Magmatic Ore Deposits and Their Application in Mineral Exploration, Short Course, Vol. 13. Geological Association of Canada, pp. 69–106.

Barnes, S.-J., Boyd, R., Korneliussen, A., Nilsson, L.-P., Often, M., Pedersen, R.-B., Robins, B., 1988. The use of mantle normalization and metal ratios in discriminating between the effects of partial melting, crystal fractionation and sulphide segregation on platinum-group elements, gold, nickel and Cu: examples from Norway. In: Prichard, H.M., Potts, P.J., Bowles, J.F.W., Cribbs, S.J. (Eds.), Geo-platinum 87 Symp. Elsevier, London, pp. 113–143.

Beauvais, A., 2009. Ferricrete biochemical degradation on the rainforest?savannas boundary of Central African Republic. Geoderma 150, 379–388.

Berger, A., Janots, E., Gnos, E., Frei, R., Bernier, F., 2015. Rare earth element mineralogy and geochemistry in a laterite profile from Madagascar. Appl. Geochem. 41, 218–228.

Bilong, P., Ndjigui, P.-D., Temdjim, R., Sababa, E., 2011. Geochemistry of peridotite and granite xenoliths under the early stages of weathering in the Nyos volcanic region (NWCameroon): implications for PGE exploration. Chem. Erde Geochem. 71, 77–86.

Bleeker, W., 1990. Thompson area-general geology and ore deposits. In Geology and Mineral Deposits of the Flin Flon and Thompson belts, Manitoba. In: Galley, A.G., Bailes, A.H., Syme, E.C., Bleeker, W., Macek, J.J., Gordon, T.S. (Eds.), Int. Assoc. Genesis of Ore Deposits Guide Book l0; Geol. Surv. Can., Open-File Rep., 2165, pp. 93–136.

Boudreau, A.E., Mathez, E.A., McCallum, I.S., 1986. Halogen geochemistry of the Stillwater and Bushveld complexes: evidence for transport of the platinum-group elements by Cl-rich fluids. J. Petrol. 27, 967–986.

Bowles, J.F.W., Gize, A.P., Melfi, A.J., 1994. The mobility of the platinum-group elements in the soils of the Freetown Peninsula, Sierra Leone. Can. Mineral. 32, 957–967.

Cabral, A.R., Beaudoin, G., Choquette, M., Lehmann, B., Polonia, J.C., 2007. Supergene leaching and formation of platinum in alluvium: evidence from Serro Minas Gerais, Brazil. Mineral. Petrol. 90, 141–150.

Campbell, I.H., Naldrett, A.J., Barnes, S.-J., 1983. A model for the origin of the platinum rich sulphide horizons in the Bushveld and Stillwater Complexes. J. Petrol. 24, 133–165.

Cawthorn, R.G., 2005. Stratiform platinum-group element deposits in layered intrusions. In: Mungall, J.E. (Ed.), Exploration for Platinum Group Element Deposits. Mineralogical Association of Canada Short Course 35, Oulu, Finland, pp. 57–73.

Champetier de Ribes, G., Aubague, M., 1956. Carte géologique de reconnaissance du Cameroun à l'échelle de 1/500 000. 0. Feuille de Yaoundé-Est + notice explicative. Dir. Mines Géol., Cameroun (35 pp).

Delvigne, J.E., 1998. Atlas of micromorphology of mineral alteration and weathering. Canad. Mineral. 3 (494 pp).

Ebah Abeng, S.A., Ndjigui, P.-D., Aye, A.B., Tessontsap, T., Bilong, P., 2012. Geochemistry of pyroxenites, amphibolites and their weathered products in the Nyong unit, SW Cameroon (NW border of Congo craton): implications for Au-PGE exploration. J. Geochem. Explor. 114, 1–19.

Fleet, M.E., Wu, T.W., 1993. Volatile mass transfer of platinum-group elements in sulfide-chloride assemblages at 1000 °C. Geochim. Cosmochim. Acta 57, 3519–3531.

Fonseca, R.O.C., Campbell, I.H., O'Neill, H.St.C., Allen, C.M., 2009. Solubility of Pt in sulphide mattes: implications for the genesis of PGE-rich horizons in layered intrusions. Geochim. Cosmochim. Acta 73, 5764–5777.

Fu, X., Wanga, J., Yuhong, Z., Tan, F., Wenbinga, C., Feng, X., 2015. The geochemistry of platinum group elements in marine oil shale-A case study from the Bilong Co oil shale, northern Tibet, China. Chem. Erde Geochem. 75, 55–63.

Ganno, S., Ngnotue, T., Kouankap, N.G.D., Nzenti, J.P., Notsa, F.M., 2015. Petrography and geochemistry of the banded iron-formations from Ntem complexes belt Elom area, Southern Cameroon: implications for the origin and depositional environment. Chem. Erde Geochem. 75, 375–387.

Ganno, S., Njiosseu, T.E.L., Kouankap, N.G.D., Djoukouo, S.A., Moudioh, C., Ngnotue, T., Nzenti, J.P., 2017. A mixed seawater and hydrothermal origin of superior-type Banded Iron Formation (BIF)-hosted Kouambo iron deposit Palaeoproterozoic Nyong series, Southwestern Cameroon: constraints from petrography and geochemistry. Ore Geol. Rev. 80, 860–875.

Godel, B., Barnes, S.-J., 2007. Platinum-group elements in sulphide minerals and the whole rocks of the J-M reef (Stillwater Complex): implication for the formation of the reef. Chem. Geol. 248 (3–4), 272–294.

Godel, B., Barnes, S.-J., Maier, W.D., 2007. Platinum-group elements in sulphide minerals, platinum-group minerals, and whole-rocks of Merensky Reef (Bushveld complex, South Africa): implications for the formation of the Reef. J. Petrol. 48, 1569–1684.

Good, D.J., Naldrett, A.J., 1993. Geology and distribution of platinum-group elements Bucko Lake intrusion. Thompson belt, Manitoba. Can. Mineral. 31, 45–60.

Goodwin, A.M., 1991. Precambrian Geology-The Dynamic Evolution of the Continental Crust. Academic Press, New York.

Grant, J.A., 1986. The isocon diagram —a single solution to Gresens' equation for metasomatic alteration. Econ. Geol. 81, 1976–1982.

Grant, J.A., 2005. Isocon analysis: a brief review of the method and applications. Phys. Chem. Earth 30, 997–1004.

Gueddari, K., Piboule, M., Amosse, J., 1994. Comportement des éléments du groupe du platine (PGE) dans les ultrabasites des Beni Bousera (Rif, Maroc): données préliminaires. C. R. Acad. Sci. Paris t 318, 79–86.

Hao, L., Zhao, X., Boorder de, H., Lu, J., Zhao, Y., Wei, Q., 2014. Origin of PGE depletion of Triassic magmatic Cu-Ni sulfide deposits in the central-southern area of Jilin province, NE China. Ore Geol. Rev. 63, 226–237.

Hsu, L.C., Lechler, P.J., Nelson, J.H., 1991. Hydrothermal solubility of palladium in chloride solutions from 300° to 700 °C: preliminary experimental results. Econ. Geol. 86, 422–428.

Ismail, S.A., Mirza, T.M., Carr, P.F., 2010. Platinum-group elements geochemistry in podiform chromitites and associated peridotites of the Mawat ophiolite, north eastern Iraq. J. Asian Earth Sci. 37, 31–41.

Lee, R.G., Dilles, J.H., Mazdab, F.K., Wooden, J.L., 2009. Europium Anomalies in Zircon from Granodirorite Porphyry Intrusions at the El Salvador Porphyry Copper Deposit, Chile. The Geological Society of America Paper n°158-8.

Lerouge, C., Cochérie, A., Toteu, F.S., Penaye, J., Milési, J.P., Tchameni, R., Nsifa, E.N., Fanning, C.M., Deloule, E., 2006. SHRIMP U-Pb zircon age evidence for Paleoproterozoic sedimentation and 2.05 Ga syntectonic plutonism in the Nyong Group, Southwestern Cameroon: consequences for the Eburnean-Transamazonian belt of NE Brazil and Central Africa. J. Afri. Earth Sci. 44, 413–427.

Lesher, C.M., Stone, W.E., 1996. Exploration geochemistry of komatiites. In: Wyman, D.A. (Ed.), Igneous Trace Elements Geochemistry, Application for Massive Sulphide Exploration, vol. 12. Geological Association of Canada, pp. 153–204 (short course notes).

Lorand, J.P., Alard, O., 2001. Platinum-group abundances in the upper mantle: new constraints from in-situ and whole rock analyses of massive central xenoliths (France). Geochim. Cosmochim. Acta 65, 2789–2806.

Manceau, A., Schlegel, M.L., Musso, M., Sole, V.A., Gauthier, C., Petit, P.E., Trolard, F., 2000. Crystal chemistry of trace elements in natural and synthetic goethite. Geochim. Cosmochim. Acta 64, 3643–3661.

Maurizot, P., Abessolo, A., Feybesse, A., Johan, J.L., Lecomte, P., 1986. Etude et prospection minières du Sud-Ouest Cameroun. Synthèse des travaux de 1978 à 1985. 85-CMR 066. BRGM.

McDonough, W.F., Sun, S.-S., 1995. The composition of the Earth. Chem. Geol. 120, 223–253.

Mountain, B.W., Wood, S.A., 1988. Chemical controls on the solubility, transport, and deposition of platinum and palladium in hydrothermal solutions: a thermodynamic approach. Econ. Geol. 83, 492–510.

Naldrett, T., Kinnaird, J., Wilson, A., Chunnett, G., 2008. Concentration of PGE in the earth's crust with special reference to the Bushveld Complex. Earth Sci. Front 15 (5), 264–297.

Naldrett, A.J., Wilson, A., Kinnaird, J., Yudovskaya, M., Chunnett, G., 2012. The origin of chromitites and related PGE mineralization in the Bushveld Complex: new mineralogical and petrological constraints. Miner. Depos. 47, 209–232.
Ndjigui, P.-D., Bilong, P., 2010. Platinum-group elements in the serpentinite lateritic mantles of the Nkamouna ultramafic massif (Lomié region, South-East Cameroon). J. Geochem. Explor. 107, 63–76.
Ndjigui, P.-D., Yongue-Fouateu, R., Bilong, P., Bayiga, E.C., Oumarou, M., 2009. Geochemical surveys of Pt, Pd and Au in talcschists and hornblendites and their weathered equivalents at Pouth-Kellé, Southern Cameroon. J. Cameroon Acad. Sci. 8, 115–128.
Neal, C.R., Taylor, L.A., 1989. A negative Ce anomaly in a peridotite xenolith: evidence for crustal recycling into the mantle or mantle metasomatism. Geochim. Cosmochim. Acta 53, 1035–1040.
Nzenti, J.P., Kapajika, B., Wörner, G., Lubala, T.R., 2006. Synkinematic emplacement of granitoïds in a Pan-African shear zone in Central Cameroon. J. Afri. Earth Sci. 45, 74–86.
Paśava, J., Vymazalov, A., Kośler, J., Koneev, R.I., Jukov, A.V., Khalmatov, R.A., 2010. Platinum-group elements in ores from the Kalmakyr porphyry Cu-Au-Mo deposit, Uzbekistan: bulk geochemical and laser ablation ICP-MS data. Miner. Depos. 45 (5), 411–418.
Penaye, J., Toteu, S.F., Tchameni, R., Van Schmus, W.R., Tchakounté, J., Ganwa, A., Minyem, D., Nsifa, N.E., 2004. The 2.1 Ga west african belt in Cameroon: extension and evolution. J. Afri. Earth Sci. 39, 1196–1202.
Prichard, H., Neary, C., Potts, P.J., et al., 1986. Platinum group minerals in the Shetland ophiolite. In: Gallagher, M.J. (Ed.), Metallogeny of Basic and Ultrabasic Rocks. Inst. Min. Metall., London, pp. 395–414.
Puchtel, H., Prichard, H.M., Berner, Z., Maynard, J., 1995. Sulfide mineralogy, sulfur content, and sulfur isotope composition of mafic and ultramafic rocks from leg 147. Proceed. Ocean Drill. Prog. Sci. Results 147, 4227–4242.
Sababa, E., Ndjigui, P.-D., Ebah Abeng, S.A., Bilong, P., 2015. Geochemistry of peridotite xenoliths from the Kumba and Nyos areas (southern part of the Cameroon Volcanic Line): implications for Au-PGE exploration. J. Geochem. Explor. 152, 75–90.
Satyanarayanan, M., Balaram, V., Sylvester, P.J., Subba Rao, D.V., Charan, S.N., Shaffer, M., Mohammed Dar, Ali, Anbarasu, K., 2011. Geochemistry of late-Archean Bhavani mafic/ultramafic complex, southern India: implications for PGE metallogeny. Appl. Geochem. 13, 1–14.
Savard, D., Barnes, S.-J., Meisel, T., 2010. Comparison between Nickel-Sulfur Fire Assay Te co-precipitation and Isotope Dilution with High-Pressure Asher acid digestion for the determination of Platinum-Group Elements, rhenium and gold. Geostan. Geoanal. Res. 34 (3), 281–291.
Shang, C.K., Satir, M., Nsifa, E.N., Liégois, J.-P., Siebel, W., Taubald, H., 2007. Archaean high-K granitoids produced by remelting of earlier Tonalite-Trondhjemite–Granodiorite (TTG) in the Sangmelima region of the Ntem complex of the Congo craton. Int. J. Earth Sci. 96, 817–841.
Shang, C.K., Liégeois, J.-P., Satir, M., Nsifa, E.N., 2010. Late Archaean high-K granite geochronology of the northern metacratonic margin of the Archaean Congo craton. Southern Cameroon: evidence for Pb-loss due to non-metamorphic causes. Gondwana Res. 18, 337–355.
Sharrad, K.A., McKinnon-Matthews, J., Cook, N.J., Ciobanu, C.L., Hand, M., 2014. The basil Cu-Co deposit, Eastern Arunta region, Northern Territory, Australia: a metamorphosed volcanic-hosted massive sulphide deposit. Ore Geol. Rev. 56, 141–158.
Shellnutt, J.G., Mab, G.S.-K., Qi, L., 2015. Platinum-group elemental chemistry of the Baima and Taihe Fe-Ti oxide bearing gabbroic intrusions of the Emeishan large igneous province. SW China. Chem. Erde Geochem. 75, 35–49.
Singh, B., Sherman, D.M., Gilkes, R.J., Wells, M.A., Mosselmans, J.F.W., 2002. Incorporation of Cr, Mn and Ni into goethite ((-FeOOH): mechanism from extended X-ray absorption fine structure spectroscopy. Clay Miner. 37, 639–649.
Song, X.Y., Keays, R.R., Zhou, M.F., Qi, L., Ihlenfeld, C., Xiao, J.F., 2009. Siderophile and chacophile elemental constraints on the origin of the Jinchuan Ni-C-(PGE) sulfide deposit, NW China. Geochim. Cosmochim. Acta 73, 404–424.
Suarez, S., Prichard, H.M., Valasco, F., Fisher, P.C., McDonald, I., 2010. Alteration of platinum-group minerals and dispersion of platinum-group elements during progressive weathering of the Aguablanca Ni-Cu deposit, SW Spain. Miner. Depos. 45 (4), 331–350.
Tchameni, R., Pouclet, A., Mezger, K., Nsifa, E.N., Vicat, J.P., 2004. Single zircon Pb–Pb and Sm-Nd whole rock ages for the Ebolowa greenstone belts: evidence for pre-2.9 Ga terranes in the Ntem Complex (South Cameroon). J. Cameroon Acad. Sci. 4, 235–246.
Teutsong, T., Bontognali, R.R.T., Ndjigui, P.-D., Vrijmoed, J.C., Teagle, D., Cooper, M., Vance, D., 2017. Petrography and geochemistry of the Mesoarchean Bikoula banded iron formation in the Ntem complex (Congo craton), Southern Cameroon: implications for its origin. Ore Geol. Rev. 80, 267–288.
Toteu, S.F., Van Schmus, W.R., Penaye, J., Nyobe, J.B., 1994. U-Pb and Sm-Nd evidence for Eburnean and Pan-African high-grade metamorphism in cratonic rocks of southern Cameroon. Prec. Res. 67, 321–347.
Traoré, D., Beauvais, A., Augé, T., Parisot, J.-C., Colin, F., Cathelineau, M., 2008. Chemical and physical transfers in an ultramafic rock weathering profile: part 2: Dissolution vs. accumulation of platinum group minerals. Amer. Miner. 93, 31–38.
Wallace, J.P., Carmichael, I.S.E., 1992. Sulfur in basaltic magma. Geochim. Cosmochim. Acta 56, 1863–1874.
Wang, Y.C., Prichard, H.M., Zhou, M.F., Fisher, P.C., 2008. Platinum-group minerals from the Jinbaoshan Pd-Pt deposit, SW China: evidence for magmatic origin and hydrothermal alteration. Miner. Depos. 41, 791–803.
Wimpenny, J., Gannoun, A., Burton, K.W., Widdowson, M., James, R.H., Gislason, S.R., 2007. Rhenium and osmium isotope and elemental behaviour accompanying laterite formation in the Deccan region of India. Earth Planet. Sci. Lett. 261, 239–258.
Xu, Y., Orberger, B., Reeves, S.J., 1998. Fractionation of platinum group elements in upper mantle: evidence from peridotite xenoliths from Wangqing. Sci. China 41 (4), 354–361.
Zaccarini, F., Proenza, J.A., Ortega-Gutiérrez, F., Garuti, G., 2005. Platinum group minerals in ophiolitic chromitites from Tehuitzingo (Acatlán complex, southern Mexico): implications for post-magmatic modification. Mineral. Petrol. 84, 147–168.
Zhou, H., McKeegan, K.D., Xu, X., Zindler, A., 2004. Fe-Al-rich tridymite-hercynite xenoliths with positive cerium anomalies: preserved lateritic paleosols and implications for Miocene climate. Chem. Geol. 207, 101–116.